A computational study of the double hysteresis phenomenon during reactive sputtering

J. Van Bever, K. Strijckmans, D. Depla

Department of Solid State Sciences, Ghent University, Krijgslaan 281 (S1), 9000 Gent, Belgium

E-mail: `Diederik.Depla@ugent.be`

April 2022

Abstract. When process parameters such as the reactive gas partial pressure or the discharge voltage are studied as a function of the reactive gas flow during reactive magnetron sputtering, the obtained curve has an S-shape. A direct consequence of this behaviour is that process control based on the reactive gas flow exhibits hysteresis. Under specific conditions, it is possible to observe two S-shaped curves: one when the reactive gas pressure is increased, the other during the return to the initial state by decreasing the reactive gas pressure. This behaviour has been described as double hysteresis behaviour. The origin of the double hysteresis behaviour is computationally studied by high-throughput calculations using a previously developed model. The influence of different process and material parameters were evaluated based on newly developed measures to characterize the calculated process curves. This high-throughput analysis reveals that the double hysteresis behaviour is linked to the difference in the removal rate of non-reacted implanted ions during the increase and decrease of the reactive gas pressure. Within the parameter space a region can be defined for which the double hysteresis behaviour is strong. The latter can not only assist further experiments to study this behaviour but also defines conditions to limit its impact. For Al, a discharge current density of approximately 0.025 A/cm^2 was found to maximize double hysteresis.

Keywords: sputtering, reactive gas, modelling

1. Introduction

Magnetron sputtering is a mature technique for thin film deposition. It is based on a magnetically enhanced gas discharge. Compound films can be deposited by sputtering from an elemental target while a reactive gas such as oxygen or nitrogen is introduced into the chamber. The reactive gas interacts not only with the deposited material but also at the target. The reaction at the target results from chemisorption of neutral species onto the target surface and from implantation of reactive ions into the target. Irrespective of the mechanism, the compound formation on the target is termed target poisoning [1]. Target poisoning can, depending on the experimental conditions, occur abruptly at a given reactive gas flow, and the return to the metallic state occurs in the same abrupt way when the flow is decreased afterwards. The transitions occur in general at different reactive gas flows. As such, hysteresis in the process curves can be observed.

If the process is controlled by the reactive gas flow and a hysteresis is observed, it is not possible to access the experimental parameter space in between the transition points. This problem is often circumvented by the application of feedback control [2]. During feedback control, a deposition parameter such as the reactive gas pressure, the deposition rate, the discharge voltage or a combination of these parameters is used to continuously control the reactive gas flow to fix the process conditions.

If the process is feedback controlled, the observed process curve, for example the reactive gas partial pressure as a function of the flow, is S-shaped. The origin of this behaviour can be explained by the interplay between the target and substrate condition which was successfully modelled by Berg *et al.* [3]. Often, however, not one but two S-shaped curves are observed, one of which corresponds to the path from the metallic to the poisoned state while the other S-shaped curve corresponds to the reverse transition [2, 4, 5].

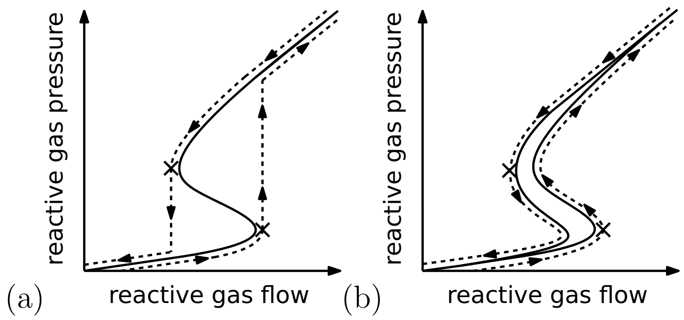

Figure 1. Process curves for single (a) and double (b) hysteresis. Depicted are the minimal model curves (full lines) and the curves that are measured without (a) or with (b) feedback control in order to observe the considered type of hysteresis experimentally (dashed lines). The crosses refer to the first (highest flow) and second (lowest flow) critical point.

A typical measuring procedure of the process curve starts from either the metallic or poisoned target state, and the controlling process parameter is changed until the process reaches the other target state. Subsequently, the controlling process parameter is again stepwise changed until the original state is reached. This slow measuring procedure implicitly includes effects which change the initial conditions. Examples are target erosion [7], target heating [8] and chamber wall heating. Also, the dynamics of the flow rate change influences the obtained process curve [9]. Therefore, a first explanation for the observation of two S-shaped curves can find its origin in these initial condition changes. For example, a different process curve will be measured for a new target as compared to a deeply eroded target. As target erosion occurs during the measurement of the process curve, two different S-shaped curves will be observed.

Measurements from Schelfhout *et al.* [10] demonstrate however that the double S-shape persists even when the aforementioned effects are excluded. Hence, the observed effect is inherent to the process. Independently of this experimental observation, the inclusion of reactive ion implantation in the theoretical description of reactive sputtering led to the prediction of a double S-shaped curve [11, 12].

As mentioned before, when the process is controlled by the reactive gas flow, only one hysteresis effect can be observed, and it is not possible to distinguish the two S-shaped curves. However, from a theoretical point of view, each S-shaped curve can be associated to a hysteresis. Therefore, in the following, the observation of a double S-shaped curve will be identified as a “double” hysteresis. To contrast with this, the hysteresis known to occur when no feedback control is applied, will be defined as “single” hysteresis. The difference between single and double hysteresis is sketched in figure 1. The minimal model curves required to predict the given type of hysteresis are also drawn in the same figure.

The observation of double hysteresis is not only important to further improve the description of the reactive sputtering process. As will be discussed in this paper, double hysteresis behaviour can be linked to the transport of non-reacted implanted ions inside the target subsurface. Diffusion of implanted species has been postulated to play an important role for HiPIMS [13, 14].

Elucidating when double hysteresis is expected to occur and in which proportions can also assist to further improve the process control. The main drive to develop feedback control of reactive sputtering is to deposit compounds at higher deposition rates by stabilization of the process between the two critical points (indicated by crosses in figure 1). With this goal, the process curve is measured in the way described before to define the parameter space of the controlling parameters. This is known as a system calibration procedure. The observation of double hysteresis complicates the feedback control procedure because the calibration procedure is only valid for one of the two S-curves.

In this paper, a high-throughput analysis of single and double hysteresis is presented. The used model and developed analysis techniques are discussed in section 2.1 and section 2.2. The results are then structured in order to identify and quantify the mechanism that causes the double hysteresis (section 3). To conclude, we discuss the required steps for a further improvement of reactive sputtering modelling.

2. Modelling and analysis techniques

2.1. RSD-model

In this work, the RSD-model developed earlier [15, 16, 11] will be used to systematically analyse the double hysteresis behaviour during reactive sputtering. The model mainly focuses on the description of target processes and how these processes contribute to the actual shape of the hysteresis curve. In this section, the main features of the model and the ingredients used for further analysis are presented. A more thorough discussion on the RSD-model can be found in previous work [15, 16, 11].

The main target processes accounted for in the model, are the following:

- Chemisorption i.e., the formation of an oxidized top layer. It is proportional to the reactive gas pressure P_{R_2} and a sticking probability α_t.
- Implantation i.e., the supply of reactive atoms to the target subsurface. Two main processes are included: direct implantation of reactive ions R_2^+ from the gas discharge and knock-on implantation of chemisorbed atoms. Direct implantation is considered to be proportional to the reactive gas fraction $f_{R_2} = P_{R_2}/P_{tot}$, with P_{tot} the total gas pressure. For the knock-on implantation, a knock-on yield β_c is introduced. The implanted species are distributed over the target depth according to a Gaussian implantation profile with mean μ and standard deviation σ, irrespective of the mechanism. A maximal implantation depth D is defined as $\mu + 3\sigma$.
- Sputtering, which results in target erosion. The latter is quantified by a surface speed v_s at which the target surface recedes. Equivalently, it is the speed at which species inside the target, such as formed compound and non-reacted implanted ions, arrive at the target surface top layer.
- The formation of a compound MR_z with fixed stoichiometry z due to the reaction of implanted ions with the target material. The reaction rate constant is denoted by k.
- Overstochiometry i.e., a limitation of the maximum concentration of reactive atoms in the target. More specifically, the current density of implanted ions is multiplied by a saturation function s which goes from 1 (no material implanted yet; maximal implantation) to 0 (maximum concentration is reached; no possibility to implant reactive gas ions further).

The above target processes are described by a set of coupled non-linear differential equations. These differential equations govern the following quantities:

- $n_M(x)$ and $n_R(x)$ correspond to the subsurface concentration of metal atoms and non-reacted reactive ions respectively, both at a depth x.
- The target surface fractions θ_m, θ_c and θ_r related to the metallic, oxidized (due to chemisorption) and reacted (after implantation) fraction, respectively.
- The reactive gas pressure P_{R_2} inside the vacuum chamber.

Furthermore, the target surface and subsurface are spatially resolved and the target fractions $\theta_{x,n}$ are considered for every cell n separately.

The resulting set of non-linear differential equations can be solved by the application of boundary conditions between the target surface and subsurface, and between the target subsurface and the bulk. The solution can be obtained either in steady-state or using a time-dependent algorithm. These algorithms are implemented in the current version (v3) of the RSD-model [17] which is freely available. The results of the high-throughput analysis were obtained using the steady-state solution method for $P_{R_2}(Q_{R_2})$ process curves, where P_{R_2} and Q_{R_2} denote the reactive gas pressure and flow respectively. Due to the non-linearity of the used equations, the RSD-model can predict a double hysteresis. Each steady-state solution thus consists of two S-shaped curves. Any point of these two curves corresponds to a unique state of the target, substrate and chamber. It is therefore possible to compare any two properties of the system and to consider distributions of properties along the curves. For a detailed discussion of the steady-state solution of the RSD-model, we refer to the work of Strijckmans [16].

From the obtained solution, the consumption rate of R_2 molecules by compound formation through the different target processes can be calculated as a reactive gas flow Q_t towards the target,

$$Q_t = (Q_{\mathrm{t,impl,dir}} + Q_{\mathrm{t,chem}}) - (Q_{\mathrm{t,erosion}} + Q_{\mathrm{t,overstoch}}) \tag{1}$$

The subsequent contributions addressed in equation (1) are the addition of reactive gas to the target due to direct implantation ($Q_{\mathrm{t,impl,dir}}$) and chemisorption ($Q_{\mathrm{t,chem}}$) and the decrease of reactive gas content of the target due to sputter erosion of non-reacted implanted ions ($Q_{\mathrm{t,erosion}}$) and a term associated with overstoichiometry ($Q_{\mathrm{t,overstoch}}$).

The RSD-model also accounts for the change in the discharge voltage due to target poisoning by including the I-V characteristic of the gas discharge with a metallic and a poisoned target. More specifically, the discharge current I and discharge voltage V are related as [18]

$$I = C_{1,i}(V - V_{0,i})^{C_{2,i}}, \tag{2}$$

with $C_{1,i}$, $V_{0,i}$ and $C_{2,i}$ empirical parameters, and this for each target surface fraction $i = m, c, r$. In general a value $C_{2,i} = 2$ is assumed. From equation (2), it follows that the target state completely determines the discharge voltage at a fixed discharge current [11]. Since also the sputter yields are connected to the discharge voltage [19], a change of the discharge current will affect through equation (2) also the sputter yield of the different materials.

2.2. Quantification of hysteresis

In order to study the influence of a certain parameter on hysteresis behavior, abstraction is made of the actual hysteresis curves. Instead, measures are chosen that quantify effects of hysteresis with a single number. These hysteresis quantification measures generally show a continuous trend as a function of process or material parameters which facilitates the interpretation.

The main hysteresis quantification techniques used for our analysis are depicted in figure 2 for different process curves. These are the following:

- *Critical points* are defined as the transition points between the metallic mode and the poisoned mode when no feedback control is applied on e.g., the reactive gas

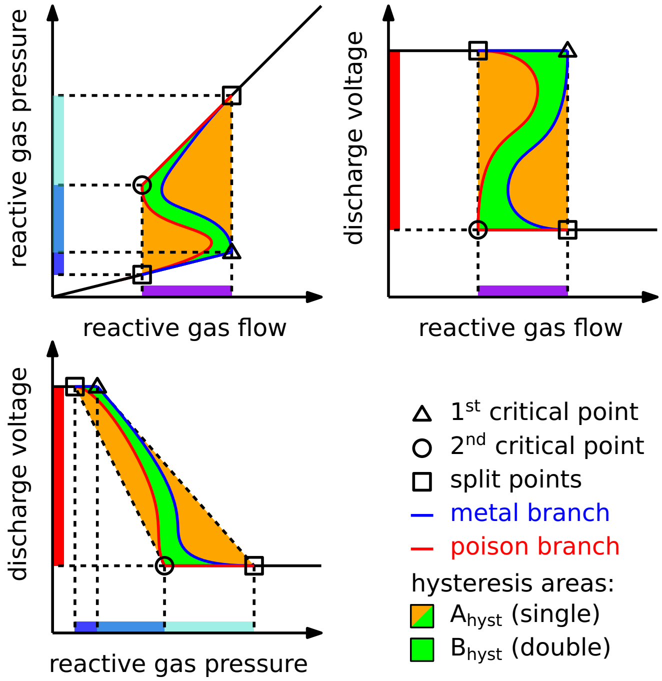

Figure 2. Definition of the main hysteresis quantification measures. The blue curve, or metal branch, is the process curve obtained when the reactive gas pressure is stepwise increased, while the red curve, or poison branch, is the process curve for a decreasing reactive gas pressure. The hysteresis curve measured during flow control is defined by two critical points. The area defined by the two critical points is A_{hyst}. The area between the two process curves, indicated in green, is B_{hyst}.

pressure. The convergence between the critical points can be used to identify the conditions for which this hysteresis behavior disappears.

- *Split points* are defined as the points at which the two S-shaped curves, observed during feedback control, separate.
- *Branch averages.* Two branches can be defined as parts of the paths for either increasing or decreasing reactive gas pressure. Properties such as the target surface fractions θ_m, θ_c, and θ_r are calculated along each branch. Hence, each branch defines a distribution for any calculated property. The mean values of these distributions can be used to monitor double hysteresis. These will be referred to as branch averages.

The branches are defined as being demarcated by the critical points and/or the split points in such a way that their extension is maximal. In figure 2, the critical points and the split points coincide and demarcate the branches. If the critical points do not exist or fall in between the split points, the branches are delimited by the split points. On the other hand, when the split points are absent or lie in between the critical points, the branches are defined to extend up to the critical points. The latter situation is of particular interest since the disappearance of double hysteresis can be properly quantified.

The branches are called the metal branch and the poison branch as shown in figure 2, since the corresponding target states tend to resemble the metallic and poisoned state respectively. The branch average of a quantity X over the metal or poison branch will be denoted by $\overline{X}\,[m]$ and $\overline{X}\,[p]$ respectively.

A last remark should be made on the sampling of the branches. In order to maximally represent the results from the $P_{R_2}(Q_{R_2})$ diagrams, a homogeneous sampling in P_{R_2} is used. Other sampling techniques slightly influence the calculated averages but do not alter the final conclusions.

- *Hysteresis areas* The integrated area between the paths when going from a pure metal target to a fully poisoned target and back can be used as a measure for the significance of the corresponding hysteresis. The area equals zero on disappearance of the hysteresis effect. On the other hand, when the area is large, significant differences can be expected between the critical point values or between the branch averaged values.

  When the paths correspond to the predicted results including feedback control (see figure 1b), the integrated area is called the double hysteresis area and will be denoted by B_{hyst}. It should be stressed that this area is in general different from the integrated area between the two critical points when flow control is used (see figure 1a). The latter area is indicated in figure 2 by A_{hyst}. Both areas can be calculated from the steady-state solution of the RSD-model.

The hysteresis quantification techniques can be applied to various types of process curves as demonstrated in figure 2. For example, the double hysteresis area B_{hyst} that is obtained from the discharge voltage V versus reactive gas pressure P_{R_2} curve (bottom figure in figure 2) turns out to be a good measure to focus the analysis on the target itself rather than on the chamber condition. This follows from the fact that the discharge voltage can be completely determined from the target state only (see section 2.1).

Averages or critical point values can be considered for any property. The analysed properties include process conditions such as gas pressures, flows and discharge voltage, but also substrate and target surface fractions as well as target subsurface fractions. Furthermore, target flows associated with effects of, for example, chemisorption and implantation can be considered separately.

To facilitate the analysis and the calculation of hysteresis quantification measures, a new software package was developed: `RSDplot`. `RSDplot` consists of a python library, a command line interface and an interactive interpreter and can process large amounts of input for and output from the RSD software [17]. The tool can be obtained on request.

2.3. High-throughput analysis

Simulations were conducted for all 34 process and material parameters of the reactive sputtering process as defined in the RSD-model. A convergence study of A_{hyst}, B_{hyst} and the critical point values was done with respect to the number of simulated steady-state pressure points ($\geqslant 1000$) and the number of target cells ($\geqslant 300$).

Next, the trends for all relevant hysteresis quantification measures were correlated with each other. It turns out that single hysteresis is represented well by A_{hyst} and that a bottom-up explanation can be provided using the critical point values. In this paper, we focus on the double hysteresis area B_{hyst} and the branch-averaged values.

A subset of parameters was observed to have a particular influence on double hysteresis, either maximizing or completely quenching it. These are: the target area A_t, the reaction rate coefficient k and the discharge current I. In case of the target area, the racetrack profile is re-scaled with A_t. The impact of these parameters on the double hysteresis behaviour was analysed in depth, which required also an analysis of the single hysteresis behaviour.

Finally, a combined study was conducted on the selected parameters and results for the double hysteresis behaviour as a function of the discharge current density J $(= I/A_t)$ were obtained. This allows the identification and quantification of the mechanism that causes double hysteresis. This mechanism is discussed in section 3.

3. Results: double hysteresis mechanism

The results are structured as following. First, a simple condition for double hysteresis is derived. This condition is discussed in section 3.1 by considering the combined influence of target area and reaction rate constant. The observed trends can be understood in terms of the discharge current density, which is treated in more depth in section 3.2. In this latter section, also the influence of the voltage dependency of the sputter yields on the magnitude of double hysteresis is discussed.

3.1. Time constants

Figure 3a depicts the double hysteresis area B_{hyst} obtained from the $V(P_{R_2})$ process curve when considering it as a function of the target area (black curve). A clear peak is observed. The peak position is almost completely independent of the type of process curve considered. For the reference system considered (appendix A) , the double hysteresis area peaks around 23 cm^2. When deviating from this value, the double hysteresis decays to zero at 0 cm^2 and around 110 cm^2 (not shown). This means that a well tuned target size and/or current density is required in order to observe double hysteresis.

Similar trends were observed for the double hysteresis area as a function of e.g., the reaction rate constant or the discharge current.

To elucidate the origin of the B_{hyst} behaviour, a simple model [12] which focuses on the balance between compound formation and sputtering during reactive ion implantation will be used to quantify the results of the high-throughput analysis. The core of this model is the same as the RSD-model i.e., the implanted reactive ions can react with the target material for a given time defined by the implantation depth and the target erosion rate.

In this simplified model, it is supposed that an initial concentration of reactive ions $n_{R,0}$ is implanted at a depth D at a time $t = 0$. The implanted ions can react with the target material during their travel towards the target surface. The concentration after a time t of reactive ions and metal atoms are denoted as $n_R(t)$ and $n_M(t)$, respectively. A second order reaction mechanism is supposed.

$$\frac{dn_M(t)}{dt} = -k\, n_M(t)\, n_R(t) \tag{3}$$

$$\frac{dn_R(t)}{dt} = -kz\, n_M(t)\, n_R(t) \tag{4}$$

If the boundary conditions $n_R(0) = n_{R,0}$ and $n_M(0) = n_{M,0}$ are applied, the solution for $n_R(t)$ from this system of differential equations is given by

$$n_R(t) = \frac{n_M(t)}{n_{M,0}} \cdot n_{R,0} \cdot \exp\left[-kt\left(zn_{M,0} - n_{R,0}\right)\right] \tag{5}$$

The time constant that follows from equation (5) is

$$\tau_k = \frac{1}{k(zn_{M,0} - n_{R,0})} \tag{6}$$

Since effects of overstoichiometry are accounted for and the reactive gas fraction typically present in the gas discharge is relatively small, the concentration of reactive gas, given by $n_{R,0}/n_{M,0}$, can be expected to be in general much smaller than z. This was confirmed by the simulation results. Hence a reasonable approximation is

$$\tau_k = \frac{1}{kz\, n_{M,0}} \tag{7}$$

This time constant is compared to the time for the implanted reactive ions to reach the target surface because, at the moment non-reacted atoms reach the surface, the reactive atoms are assumed to return to the gas phase. The time to reach the surface is given by D/v_s, with v_s the surface speed and D the maximal implantation depth (see section 2.1). In the following, the averaged value of the metal and poison branch are considered.

$$\tau_m = \overline{D/v_s}\,[m] \qquad \tau_p = \overline{D/v_s}\,[p], \tag{8}$$

where the character between square brackets indicate that the average is taken of samples from the metal (m) or poison (p) branch, respectively.

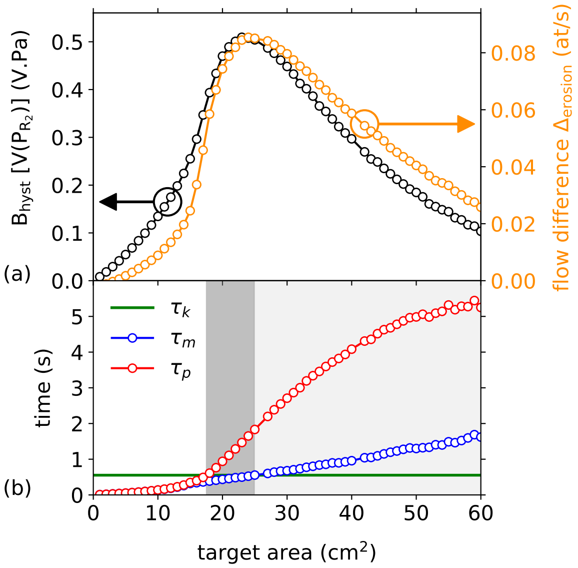

Figure 3. (a) The double hysteresis area B_{hyst} (black) and the flow difference $\Delta_{\mathrm{erosion}}$ (orange) as a function of the target area. Simulations were performed with the parameters from appendix A, excluding the target area. (b) The time constant for the chemical reaction τ_k (green) and the time to reach the target surface for the metal branch τ_m (blue) or for the poison branch τ_p (red) as a function of the target area. The grey regions demarcate the conditions discussed in the text.

In figure 3b, the reaction time constant τ_k (equation (7)) is plotted together with the erosion times τ_m and τ_p (equation (8)). Three different regimes, indicated in grey, can be distinguished.

- For large target areas, it is observed that $\tau_k < \tau_m < \tau_p$. This means that most of the implanted material reacts before it reaches the target surface, and this situation holds for both branches. For large target areas, the ion current density, and hence the erosion rate, is small which provides sufficient time for the ions to react with the target material before they leave the target.
- For very small target areas, one has $\tau_m \approx \tau_p < \tau_k$. In this regime the ion current density is high, so that almost no reaction takes place neither for the metal or poison branch. Most of the implanted reactive ions reach the target surface and return to the gas phase without reaction.
- An intermediate regime for which $\tau_m < \tau_k < \tau_p$. Here, a different situation is observed for the metal and poison branch. In the former case, the implanted reactive gas ions leave the target mainly non-reacted while in the latter case the implanted ions mainly react.

The double hysteresis area is observed to peak in the regime for which $\tau_m < \tau_k < \tau_p$. The spreading of the peak of $B_{\mathrm{hyst}}[V(P_{R_2})]$ beyond the boundaries for which $\tau_k = \tau_m$ or $\tau_k = \tau_p$ can be attributed to the implied assumptions. Not all reactive gas ions are implanted at a depth D, but they are distributed according to the implantation profile.

Also, the branch averaged values were taken, while in fact each branch corresponds to a distribution of target states.

The above analysis indicates that the double hysteresis area is related to the possibility for the implanted ions to react within the time interval defined by their implantation and their removal by sputter erosion. It is therefore expected that the difference between the branch averages of $Q_{\mathrm{t,erosion}}$ (equation (1)), or thus

$$\Delta_{\mathrm{erosion}} = \overline{Q_{\mathrm{t,erosion}}}\,[m] - \overline{Q_{\mathrm{t,erosion}}}\,[p], \tag{9}$$

is a better measure for the magnitude of the double hysteresis, because it describes the difference in rate at which the non-reacted implanted reactive ions leave the target by sputter erosion in both branches.

In figure 3a, the values of $\Delta_{\mathrm{erosion}}$ (equation (9)) are shown (orange curve). A good correspondence with $B_{\mathrm{hyst}}[V(P_{R_2})]$ is found. Good correspondence was also obtained when simulations were performed as a function of other parameters than the target area.

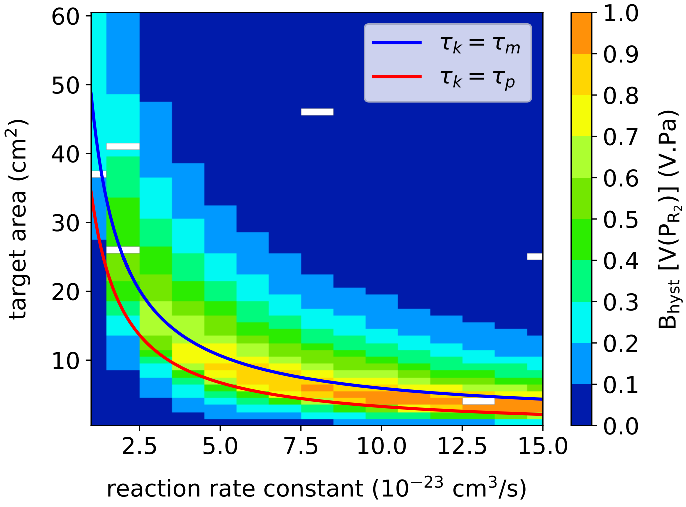

Figure 4. $B_{\mathrm{hyst}}[V(P_{R_2})]$ as a function of the target area and the reaction rate constant. Simulations were performed with the parameters from appendix A, excluding the varied parameters. Combinations of the target area and the reaction rate constants for which no convergence was obtained in the RSD model are indicated in white. Also shown are the conditions that fulfil the requirement $\tau_k = \tau_m$ (blue line) or $\tau_k = \tau_p$ (red line). τ_k is the time constant for the chemical reaction as defined in equation (7), while τ_m and τ_p (equation (8)) are the average times for the implanted reactive ions to reach the target surface in the metal and poison branch, respectively. It can be observed that the double hysteresis area is maximal between the two conditions, except for the combination of a low reaction rate constant and a large target area.

To study this hypothesis further, the same analysis was performed multiple times, each time for a different value of the reaction rate constant k. This corresponds to the naive idea of shifting the horizontal (green) line for τ_k in figure 3b in the vertical direction by a change of k, so that the boundaries for which $\tau_k = \tau_m$ or $\tau_k = \tau_p$ shift too. In figure 4, $B_{\mathrm{hyst}}[V(P_{R_2})]$ is plotted as a function of the target area and the reaction rate constant. A similar figure for $\Delta_{\mathrm{erosion}}$ (not shown) is obtained. It is observed that the peak of $B_{\mathrm{hyst}}[V(P_{R_2})]$ almost always falls within the region for which $\tau_m < \tau_k < \tau_p$. This confirms that double hysteresis can be attributed to the difference in sputter removal of non-reacted implanted ions between the metal and the poison branch, and that the time constants in equation (7) and equation (8) provide good measures to estimate the regime for which this difference is maximal.

3.2. Scaling

The target erosion defines the time allocated to the reactive implanted ions to react with the target material. The target erosion is defined by the target sputter yield, and the (ion) current density. In the previous section, the latter was modified by a change of the target area. This study is expanded by calculating the double hysteresis area for multiple combinations of the target area and the discharge current. This is depicted in figure 5.

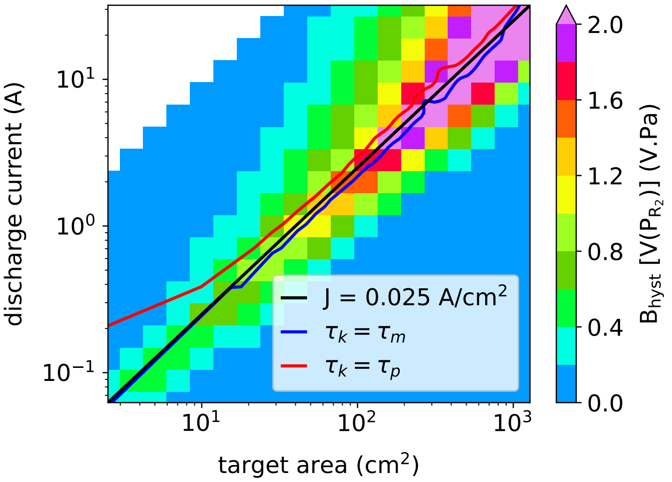

Figure 5. $B_{\mathrm{hyst}}[V(P_{R_2})]$ as a function of the target area and the discharge current. Simulations were performed with the parameters from appendix A, excluding the varied parameters. Besides, the sputter yields were kept constant: $Y_m = 0.65$ and $Y_c = Y_r = 0.02$ [20, 21]. The white region corresponds with simulations for which no convergence was obtained. Also depicted are the lines for which τ_k (equation (7)) equals either τ_m or τ_p (equation (8)). A constant discharge current density $J = 0.025$ A/cm^2 is indicated (black line). Further discussion is found in the text.

It is observed that, when either fixing the target area or the discharge current, a maximal double hysteresis is obtained at a fixed value of the discharge current density, which is indicated by the black line in figure 5.

However, a clear increase of B_{hyst} is observed when the target area and the discharge current are increased simultaneously. As discussed by Berg *et al.* [1], increasing the current results in a magnification or scaling of the hysteresis due to the fact that more material is deposited, and hence more reactive gas is consumed. An additional effect arises here from the discharge voltage. When the discharge current is increased, the discharge voltage changes accordingly (equation (2)). The I-V characteristic depends on the target condition. With the used parameters, a steeper I-V characteristic is assumed for the poisoned target. As a consequence of this, the $V(P_{R_2})$ process curve is stretched along the V-axis and a broader double hysteresis is observed.

From figure 5, a particular value of $J = 0.025$ A/cm^2 is found to maximize double hysteresis. At this discharge current density, the condition $\tau_m < \tau_k < \tau_p$ is always fulfilled. The value of $J = 0.025$ A/cm^2 is generic for the assumed target material (Al), but different values are expected to be obtained for other target materials. Indeed, the condition $\tau_m < \tau_k < \tau_p$ depends to a large extend on material dependent parameters such as the sputter yields and the reaction rate constant. Furthermore, some target materials result in steeper I-V characteristics for the metallic target rather than for the poisoned target. A broad investigation on material dependencies should be subjected to future research.

In the above analysis, the sputter yield dependency on the discharge voltage was not included. It is however known that the yields vary with the discharge voltage [19]. Figure 6 compares $B_{\text{hyst}}[V(P_{R_2})]$ as a function of the discharge current. The sputter yields, which approximately have a dependency of the form [19]

$$Y_x = Y_{x,a} \cdot V + Y_{x,b} \tag{10}$$

are either assumed to be constant ($\mathrm{Y}_{x,a} = 0$) or to be discharge voltage dependent ($\mathrm{Y}_{x,a} \neq 0$). In the former case, the values $Y_m = 0.65$ and $Y_c = Y_r = 0.02$ from literature are used [20, 21]. In the latter case, the values of appendix A are applied.

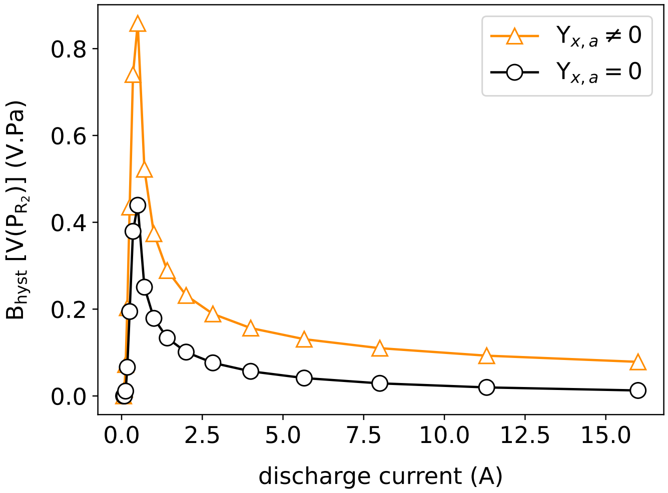

Figure 6. $B_{\text{hyst}}[V(P_{R_2})]$ as a function of the discharge current. The values are obtained with a constant sputter yield ($\mathrm{Y}_{x,a} = 0$, circles) or a sputter yield that depends on the discharge voltage ($\mathrm{Y}_{x,a} \neq 0$, triangles). Other parameters are taken from appendix A.

A more pronounced double hysteresis is observed when the sputter yield increases with the discharge current. As discussed above, a higher deposition rate results in more reactive gas consumption and a wider hysteresis behavior. Two additional effects occur which directly affect the erosion difference of non-reacted implanted ions. First, the voltage dependency of the compound sputter yield is less strong as for the metal sputter yield. This leads to an increased difference in erosion rate between the metal and poison branch. Similarly, the I-V characteristics of the gas discharge with the poisoned target is much steeper. Therefore, the discharge voltage and consequently the compound sputter yield increase less strong with increasing discharge current for the poison branch. This again induces the difference in erosion rate to increase.

When the voltage dependency of the sputter yields is included, the region of maximized double hysteresis does no longer coincide with a region of constant discharge current density as was observed for the constant sputter yield simulations (figure 5). The correct trend (not shown) slightly deviates and is defined by a line at a fixed branch average $\overline{v_s}\,[m] \approx \overline{v_s}\,[p]$ of the surface speed v_s (see section 2.1). A value of approximately 8 nm/s was found.

4. Discussion

The results from section 3.1 and section 3.2 can be understood in terms of a single mechanism. The simulations show that double hysteresis is linked with the removal rate of non-reacted species from the target by sputtering. In the metal branch i.e., when increasing the reactive gas partial pressure, the erosion rate is high, and the critical concentration to form a subsurface compound layer is reached at higher reactive gas pressures. Due to the low erosion rate in the poison branch, the reactive gas partial pressure must be reduced to a lower value as compared to the metal branch to return to the metal state in the subsurface region. This difference in target state can be observed better in the $V(P_{R_2})$ process curves since the target state and the discharge voltage are directly connected via the I-V characteristics. For the typical $P_{R_2}(Q_{R_2})$ process curves, the differences in target condition and discharge voltage result in a difference in sputtering, and hence in a difference in reactive gas consumption. So, although the aforementioned mechanism also underlies the double hysteresis from the $P_{R_2}(Q_{R_2})$ process curves, these curves are expected to be a less useful probe for double hysteresis as for example the voltage dependency of the sputter yields acts in a complicated way on both the subsurface mechanism as directly on the reactive gas consumption.

The simulations indicate that target related properties such as discharge current density (or target area or discharge current) directly affect the subsurface mechanism. The discharge current density influences the time the implanted reactive gas ions have to react before they reach the target surface, and are subsequently removed from the target by sputtering. More specifically, the size of the double hysteresis could be related to the rate of implanted reactive ions that escape from the target before reaction in the metal to poison transition but not in the poison to metal transition. A well-suited combination of the target parameters is required to induce this difference. In the particular case of Al, this occurs at a discharge current density of about 0.025 A/cm^2 or more precisely at a branch averaged surface speed of 8 nm/s.

The target material dependency of the discussed mechanism is connected to the reaction rate constant k and the sputter yields of both compound and metal. At this point, the reaction rate constant cannot be predicted and is only obtained by fitting experiments [16]. The reaction rate constant accounts only for the formation of the compound, but not for competing reverse reactions. Experimentally, the formation of nitrogen molecules during bombarding of InN, GaN, and BN has been demonstrated at ion energies similar to magnetron sputter conditions, but for much lower current densities [22, 23].

Another point which is not included in the model and which will affect the value of k, is the diffusion of implanted ions. Measurements [24, 25, 26, 20] indicate the possible role of out-diffusion of implanted ions during DC reactive magnetron sputtering and ion beam sputtering. It remains however difficult to investigate this diffusion and its exact influence on the reactive sputtering process. The RSD-model, as formulated in section 2.1, does not contain a real diffusive term. To compensate for this deficit, an overstoichiometry flow (see equation (1)) was introduced to avoid excessive implanted concentrations. In section 3.1, the target flow due to erosion of non-reacted implanted ions was used to obtain a measure for double hysteresis (see equation (9)). A similar fit can however be obtained when using $Q_{\mathrm{t,erosion}} - Q_{\mathrm{t,overstoch}}$ instead of $Q_{\mathrm{t,erosion}}$, and a good agreement is found with the trends from $B_{\mathrm{hyst}}[V(P_{R_2})]$. This is also more generally true. From this, the effect of double hysteresis seems to be reduced by the amount of reactive gas that escapes by overstoichiometry. This sounds reasonable: if the overstoichiometry flow is maximized by setting the saturation function $s = 1$, any implanted ion escapes directly from the target. In this limit no implanted material is added to the target subsurface and consequently no contribution to the sputter removal of non-reacted ions is done. A similar reasoning might apply for effects of out-diffusion. This out-diffusion is expected to increase with the concentration of non-reacted implanted ions and to become considerable before effective overstoichiometry is encountered. From this, a narrowing of the predicted double hysteresis towards poisoning is expected, which would considerably improve the quantitative prediction of the shapes of double hysteresis curves obtained so far. More experiments that explicitly target double hysteresis should be conducted however to verify the latter hypothesis. Apart from the dependency on the implanted concentration, out-diffusion is expected to increase with temperature. This might be measured directly from the size of the double hysteresis for varying temperatures, for which a slight increase is predicted when no out-diffusion is considered.

5. Conclusion

A quantitative method to analyse hysteresis behaviour during reactive magnetron sputtering was introduced. This method is based on the usage of measures that quantify properties of the hysteresis curves with a single number. The introduced measures can be linked to physical changes of the hysteresis curve and demonstrate continuous trends as a function of process and material parameters. A software package was developed and is available on request.

These measures are not only interesting from a simulation point of view, but can also be used to quantify hysteresis behavior observed in experiments.

A set of high-throughput calculations was conducted using a state-of-the-art code for predictions on hysteresis curves. The analysis was focused on the identification and quantification of the mechanism that causes double hysteresis. Double hysteresis was found to be related to the difference of the sputter removal of non-reacted implanted ions between the metal to poison and the poison to metal transition. From this, it follows that a well-suited combination of target conditions such as the target area, reaction rate constant and discharge current is required to observe a double hysteresis. For Al, a discharge current density of approximately 0.025 A/cm^2 was found. These observations can be used to omit double hysteresis when encountered during process control. Alternatively, the formulas and fits behind it could be used to study more complicated effects during reactive magnetron sputtering. This was discussed for the case of out-diffusion of non-reacted implanted ions. It is expected that this out-diffusion will further improve the predicted trends.

Acknowledgments

The authors wish to acknowledge Ghent University for the financial support through the project TIMERS (grant number 01J05319). The main author would like to thank his family and loved ones for always supporting him.

A. Reference system

A reference system was obtained from fig. 14 and appendix B of Strijckmans *et al*, [11] where experimental data for an Al/O$_2$-system had been fitted. A minor correction was applied for the racetrack and experimental data for the secondary electron yield [27] were included. The data was refitted using the compound sputter yield and the effective substrate surface area. The fit successfully reproduces the experimental data for different pumping speeds [11]. The newly fitted compound sputter yield remains in good agreement with experimental data from Schelfhout *et al* [21, 20]. The parameters are enlisted in table 1.

Table 1. reference used for parameter scans

simulation parameter	**symbol**	**value**
discharge current (A)	I	0.5
pumping speed (l/s)	S	65.43
argon pressure (Pa)	P_{Ar}	0.4
gas temperature (K)	T	300
Discharge current with metal/chemisorbed target (A)	$I_{\mathrm{m/c}}$	$2.55 \cdot (V - 260)^2 \cdot 10^{-5}$
Discharge current with reacted target (A)	I_{r}	$3.13 \cdot (V - 245)^2 \cdot 10^{-4}$
molar mass of reactive gas (O_2) (g/mol)	M_{R}	32
molar mass of target metal (Al) (g/mol)	M_{M}	26.98
mass density of target metal (Al) (g/cm^3)	ρ_{M}	2.702
sputter yield non-reacted material (M particle/ion)	Y_{m}	$(1.91 \cdot V - 111) \cdot 10^{-3}$
sputter yield reacted/chemisorbed material (MR$_z$ particle/ion)	$Y_{\mathrm{r/c}}$	$(0.049 \cdot V + 5) \cdot 10^{-3}$
secondary electron yield for non-reacted/chemisorbed material (electrons/ion)	$\gamma_{e,m/c}$	0.09
secondary electron yield for reacted material (electrons/ion)	$\gamma_{e,r}$	0.19
stoichiometric factor z for MR$_z$	z	1.5
reaction rate constant for implanted reactive atom (cm^3/(s·atom)	k	$1.95 \cdot 10^{-23}$
molecular sticking coefficient of reactive gas on substrate/target	$\alpha_{s/t}$	0.1
knock-on yield of chemisorbed/reacted atoms (R atoms/ion)	$\beta_{c/r}$	0.2/0
gaussian implantation profile with mean/deviation (nm)	μ/σ	1/0.5
saturation limit and spread of implanted reactive gas	L/S	1.1/0.05
gaussian target current profile with mean/deviation (cm)	μ_c/σ_c	1.03/0.28
total area of target/substrate (cm^2)	$A_{t/s}$	20/7100
redeposition fraction	ϵ_r	0

References

[1] Berg S, Särhammar E and Nyberg T 2014 *Thin Solid Films* **565** 186–192

[2] Sproul W D, Graham M E, Wong M S and Rudnik P J 1997 *Surface and Coatings Technology* **89** 10–15

[3] Berg S and Nyberg T 2005 *Thin Solid Films* **476** 215–230

[4] Sproul W D, Christie D J and Carter D C 2005 *Thin Solid Films* **491** 1–17

[5] Aiempanakit M, Kubart T, Larsson P, Sarakinos K, Jensen J and Helmersson U 2011 *Thin Solid Films* **519** 7779–7784

[6] Depla D, Strijckmans K and Gryse R D 2014 *Surface and Coatings Technology* **258** 1011–1015

[7] Bondarenko A, Kolomiytsev A and Shapovalov V 2016 *Journal of Physics: Conference Series* **729** 012006

[8] Kubart T, Kappertz O, Nyberg T and Berg S 2006 *Thin Solid Films* **515** 421–424

[9] Schelfhout R, Strijckmans K and Depla D 2016 *Applied Physics Letters* **109** 111605

[10] Strijckmans K, Schelfhout R and Depla D 2018 *Journal of Applied Physics* **124** 241101

[11] Depla D, Mahieu S and De Gryse R 2008 Depositing aluminium oxide: a case study of reactive magnetron sputtering *Reactive Sputter Deposition* (*Springer series in materials science* vol 109) (Springer) chap 5, pp 153–197

[12] Brenning N, Gudmundsson J T, Raadu M A, Petty T J, Minea T and Lundin D 2017 *Plasma Sources Science and Technology* **26** 125003

[13] Gudmundsson J T, Lundin D, Raadu M A, Petty T J, Minea T M and Brenning N 2018 On recycling in high power impulse magnetron sputtering discharges *2018 IEEE International Conference on Plasma Science (ICOPS)* (IEEE)

[14] Strijckmans K and Depla D 2014 *Journal of Physics D: Applied Physics* **47** 235302

[15] Strijckmans K 2015 *Modeling the reactive magnetron sputtering process* dissertation Ghent University

[16] 2021 The RSD software can be freely downloaded from `www.draft.ugent.be`

[17] Westwood W D, Maniv S and Scanlon P J 1983 *Journal of Applied Physics* **54** 6841–6846 ISSN 0021-8979 publisher: American Institute of Physics

[18] Depla D 2014 *Nuclear Instruments and Methods in Physics Research Section B: Beam Interactions with Materials and Atoms* **328** 65–69 ISSN 0168-583X

[19] Schelfhout R, Strijckmans K and Depla D 2018 *Journal of Physics D: Applied Physics* **51** 155202

[20] Schelfhout R, Strijckmans K and Depla D 2020 *Surface and Coatings Technology* **399** 126097

[21] Petravic M, Majlinger Z, Bozanic A, Yang Y W, Gao M and Crotti C 2008 Characterisation of nitrogen-related defects in compound semiconductors by near-edge x-ray absorption fine structure *Conference on Optoelectronic and Microelectronic Materials and Devices COMMAD* pp 98–100 ISBN 1097-2137

[22] Peter R, Bozanic A, Petravic M, Chen Y, Fan L J and Yang Y W 2009 *Journal of Applied Physics* **106** 083523 ISSN 0021-8979

[23] Espy S L, Urazgildin I F, Barnes A V, Yao Y, Allen J L, Albridge R G and Tolk N H 1993 Low-energy sputtering yield measurement of O^+, O_2^+, N^+, and N_2^+ incident on al and Al_2O_3 surfaces *Damage to Space Optics and Properties and Characteristics of Optical Glass* (*Proceedings of the society of photo-optical instrumentation engineers (SPIE)* vol 1761) ed Breckinridge J and Marker A (Soc Photo Opt Instrumentat Engineers) pp 130–140

[24] Depla D, Colpaert A, Eufinger K, Segers A, Haemers J and De Gryse R 2002 *Vacuum* **66** 9–17

[25] Janssens T and Vandervorst W 2007 *Surface Science* **601** 763–771

[26] Depla D, Mahieu S and De Gryse R 2009 *Thin Solid Films* **517** 2825–2839 ISSN 0040-6090